# Automatic MTPA Control for IPMSM Drives Based on Pseudorandomly Reversed Fixed-Frequency Sinusoidal Signal Injection

Ke Li, Tianfu Sun, *Senior Member, IEEE*, Jianing Liang, Mikail Koc, and Yimin Zhou, *Member, IEEE*

***Abstract*—Signal-injection-based methods are a kind of competitive maximum torque per ampere (MTPA) control schemes for interior permanent magnet synchronous motor drives, due to their motor parameter independence and satisfactory control performance. However, the high current spectrum peaks (CSPs) produced by the conventional fixed-frequency injected signals may cause negative effects. To deal with this problem, an MTPA control method based on pseudorandomly reversed fixed-frequency (PRRFF) sinusoidal signal injection is proposed in this article. The PRRFF sinusoidal signals are injected into the *d*- and *q*-axis currents via a specific current loop, and the MTPA operating points can be detected utilizing the resultant system response. Benefiting from the random characteristic of the injected signals, the proposed method can achieve far lower injection-induced CSPs than the conventional fixed-frequency injection methods. Moreover, benefiting from the fixed-frequency characteristic of the injected signals, the proposed method avoids the difficult matching of candidate injection frequencies that exists in the pseudorandom-frequency injection method. The validity of the proposed method is confirmed by experiments.**

***Index Terms*—Current spectrum peaks (CSPS), interior permanent magnet synchronous motor (IPMSM) drives, maximum torque per ampere (MTPA) control, motor parameter variations, signal injection.**

Manuscript received 28 December 2022; revised 11 June 2023; accepted 19 July 2023. Date of publication 18 August 2023; date of current version 29 February 2024. This work was supported in part by the Natural Science Foundation of Guangdong Province under Grant 2023A1515030112, in part by the National Natural Science Foundation of China under Grant 51707191, in part by Shenzhen Science and Technology Program under Grant JSGG20210629144805018 and Grant KQTD2017033016491218, and in part by Youth Innovation Promotion Association of the Chinese Academy of Sciences under Grant 2021360. *(Corresponding author: Tianfu Sun.)*

Ke Li, Tianfu Sun, Jianing Liang, and Yimin Zhou are with the Shenzhen Institutes of Advanced Technology, Chinese Academy of Sciences, Shenzhen 518055, China (e-mail: ke.li1@siat.ac.cn; tf.sun@siat.ac.cn; jn.liang@siat.ac.cn; ym.zhou@siat.ac.cn).

Mikail Koc is with the Engineering Faculty, Kirsehir Ahi Evran University, 40100 Kirsehir, Turkey (e-mail: mkoc@ahievran.edu.tr).

Color versions of one or more figures in this article are available at https://doi.org/10.1109/TIE.2023.3301523.

Digital Object Identifier 10.1109/TIE.2023.3301523

## I. Introduction

NOWADAYS, energy saving has become an important concern, especially for electric drive systems. As a kind of high efficiency motors with attractive features, interior permanent magnet synchronous motors (IPMSMs) are increasingly used in various applications [1]. For an IPMSM, both the *d*- and *q*-axis currents can produce electromagnetic torque, and the *d*- and *q*-axis current combination for a given torque is not unique [2]. To generate the required torque with low system losses, maximum torque per ampere (MTPA) control strategy is a preferred solution to distribute the *d*- and *q*-axis currents, with which the stator current magnitude can be minimized.

For decades, plenty of efforts have been made to realize MTPA control [3]. The most common practice is to calculate the current/flux references online with the MTPA analytical solution derived from motor mathematical model [4], [5], [6], [7], [8], [9], [10]. In order to deal with the challenge posed by motor parameter variations, the motor parameters involved in the MTPA analytical solutions are usually obtained from prior knowledge or online estimation. However, as pointed out in [10] and [11], most of this kind of methods neglect the derivatives of motor parameters with respect to the current vector angle (or *d*- and *q*-axis currents), and thus, the MTPA control accuracy needs to be enhanced. The search-based methods, which search the MTPA voltage/current references online, can avoid the above-mentioned problem due to the dependence of motor parameters [12]. Nevertheless, it is a great challenge for this kind of methods to balance the dynamic and steady-state performance.

In addition to the search-based methods, the signal-injection-based methods are another kind of parameter-independent MTPA control methods [13], [14], [15], [16], [17], [18]. By injecting special high-frequency (HF) signals into the motor, this kind of methods can detect the MTPA operating points according to the resultant system responses such as torque [13], speed [14], electric power [16], and dc-link current [18]. The signal-injection-based methods, benefiting from the high injection frequency and parameter independence, can realize an MTPA control with satisfactory accuracy and dynamic performance. In these methods, the injected signals are often repeatable fixed-frequency signals, and the induced HF components in

motor phase currents are concentrated at certain frequencies. In this case, high current spectrum peaks (CSPs) are inevitably introduced, which may result in electromagnetic interference and even audible noise problems [19].

In recent years, the virtual-signal-injection-based methods were reported, which mathematically inject the desired signals into current vector angle and then detect the MTPA operating points according to the virtual system response [20], [21], [22], [23], [24], [25]. This kind of methods could avoid the possible negative effects caused by the injected signals. However, due to the absence of real signal injection, such methods neglect the derivatives of motor parameters with respect to the current vector angle, and additional offline tests [11] or online estimation [26] is necessary to improve the MTPA control accuracy at high current amplitude.

The abovementioned discussions show that among various MTPA control methods, the signal-injection-based methods have relative technical superiority due to their motor parameter independence and satisfactory control performance, but the high injection-induced CSPs may result in negative effects. The pseudorandom signal injection techniques used in sensorless control may provide reference for reducing the injection-induced CSPs in MTPA control. In [27] and [28], the pseudorandom-frequency sinusoidal signals were served as the injected signals for sensorless control, and the injection-induced current spectrums were expanded, reducing the CSPs. Subsequently, the pseudorandom square-wave signal injection methods were investigated [19], [29], [30], [31], [32], [33], [34], where the random characteristics of the injected signals often manifest in frequency, phase, action time, or frequency-and-phase. In [35], the switching between the candidate injected signals follows a Markov chain, and the CSP reduction effect was improved. In addition, the pseudorandom triangular-wave signal injection was also adopted in sensorless control [36], which can realize lower injection-induced CSPs compared with the fixed-frequency triangular-wave and square-wave signal injection methods.

In [37], the idea of pseudorandom signal injection was introduced in MTPA control through the pseudorandom-frequency sinusoidal current injection, and a relatively satisfactory effect of CSP reduction was achieved. Nevertheless, this method involves the matching of the candidate injection frequencies for randomly varying, and it is difficult to find the frequency matching that meets both the signal-to-noise ratio (SNR) and CSP reduction requirements.

In this article, a novel signal-injection-based MTPA control method for IPMSM drives is proposed. Unlike the existing methods, the proposed method employs the pseudorandomly reversed fixed-frequency (PRRFF) sinusoidal signal as the injected signal. Benefiting from the random characteristic of the injected signal, this method can realize an MTPA control with low injection-induced CSPs. Additionally, the presented method inherits the advantage of the fixed-frequency injection methods, which can avoid the difficult candidate injection frequency matching that exists in the pseudorandom-frequency injection method. The performance of the proposed method is experimentally evaluated on an IPMSM drives.

## II. Preliminary Knowledge for MTPA Control

To facilitate the analysis of the MTPA control for IPMSM drives, the mathematical model of an IPMSM can be established in the $d$-$q$ synchronously rotating reference frame, as follows:

$$u_d = Ri_d + L_d\frac{di_d}{dt} - \omega_e L_q i_q \tag{1}$$

$$u_q = Ri_q + L_q\frac{di_q}{dt} + \omega_e L_d i_d + \omega_e \psi_f \tag{2}$$

$$T_e = \frac{3p}{2}\left[\psi_f i_q + (L_d - L_q)\, i_d i_q\right] \tag{3}$$

where $u_{d,q}$, $i_{d,q}$, and $L_{d,q}$ are the $d$- and $q$-axis voltages, currents, and inductances, respectively; $R$, $\omega_e$, $\psi_f$, $p$, and $T_e$ are the stator resistance, electrical angular speed, permanent magnet flux linkage, number of pole pairs, and electromagnetic torque, respectively.

It follows from (3) that, the current operating point $(i_d, i_q)$ that can generate a given torque is not unique. Among these operating points, there exists an operating point with the minimum current magnitude, i.e., the MTPA point. A common way to obtain the MTPA points is calculating with (4). It should be pointed out that the current operating points calculated by (4) are not the actual MTPA points, because the motor parameter variations are not fully considered in the derivation of this equation [11]

$$i_d = \frac{\psi_f}{2\,(L_q - L_d)} - \sqrt{\frac{\psi_f^2}{4(L_q - L_d)^2} + i_q^2}. \tag{4}$$

According to [18], the actual MTPA points can be regarded as solutions to the following constrained optimization problem:

$$\text{minimize } |i_s| = \sqrt{i_d^2 + i_q^2}, \text{ subject to } T_e = T_{e0} \tag{5}$$

where $|i_s|$ is the magnitude of the stator current, and $T_{e0}$ is the desired torque. By implementing the Lagrange multiplier method, the MTPA condition $i_d(\partial T_e/\partial i_q) - i_q(\partial T_e/\partial i_d) = 0$ can be derived from (5). For ease of discussion, let

$$F = i_d\frac{\partial T_e}{\partial i_q} - i_q\frac{\partial T_e}{\partial i_d}. \tag{6}$$

Then, the derived MTPA condition $i_d(\partial T_e/\partial i_q) - i_q(\partial T_e/\partial i_d) = 0$ can be summarized as $F = 0$.

It is worth noting that $F$ is closely related to the operating point of the system, as shown in Fig. 1 [18]. It can be seen that $F$ reflects the relative location between the operating point and the MTPA point, and satisfies $F = 0$ at the MTPA point. Thanks to this characteristic, $F$ can be served as an *MTPA indicator*. In this case, an accurate MTPA control can be achieved by forcing $F$ to zero, i.e., $F = 0$.

## III. Proposed MTPA Control Strategy Based on PRRFF Sinusoidal Signal Injection

In this section, a novel MTPA control method using PRRFF sinusoidal signal injection is proposed to realize an MTPA operation with reduced injection-induced CSPs.

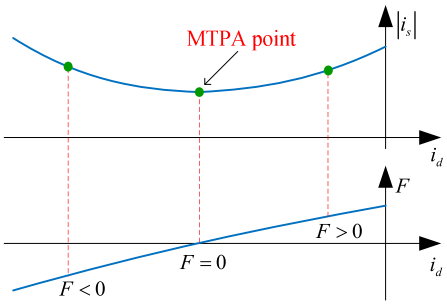


Fig. 1. Schematic diagram of the typical $i_d$–$|i_s|$ and $i_d$–$F$ characteristic curves under constant torque.

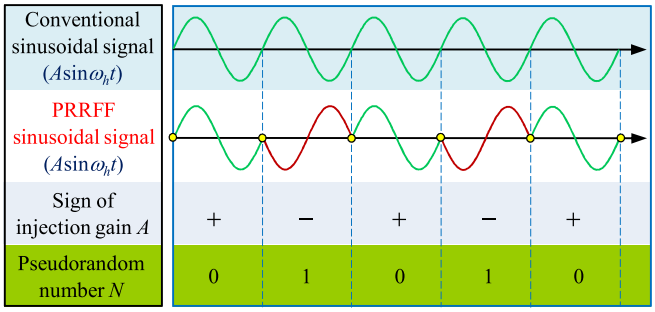


Fig. 2. Principle of the PRRFF sinusoidal signal generation.

## A. PRRFF Sinusoidal Signal for Injection

The sinusoidal signal for injection can be uniformly expressed as $A\sin\omega_h t$, where $A$ and $\omega_h$ denote the injection gain and injection frequency, respectively. In the conventional signal-injection-based MTPA control methods, the injection frequency $\omega_h$ and injection gain $A$ are usually constant, i.e., the sinusoidal signal for injection is repeatable. This makes the induced HF components in motor currents to be concentrated at certain frequencies, resulting in unwanted high CSPs. To deal with this problem, a PRRFF sinusoidal signal with random characteristic is investigated and adopted in the proposed method. This signal is generated by pseudorandomly reversing the conventional fixed-frequency sinusoidal signal, i.e., pseudorandomly reversing the sign of the injection gain $A$.

The principle of the PRRFF sinusoidal signal generation is illustrated in Fig. 2. It can be seen that the PRRFF sinusoidal signal is determined by a pseudorandom number $N$ with the value of 0 or 1; if $N = 0$, the conventional (positive gain) sinusoidal signal is served as the PRRFF sinusoidal signal, i.e., the injection gain $A$ of the PRRFF sinusoidal signal is positive; if $N = 1$, the reversed conventional sinusoidal signal is served as the PRRFF sinusoidal signal, i.e., the injection gain $A$ of the PRRFF sinusoidal signal is negative; once a (or other preset number of) sinusoidal cycle is finished, the pseudorandom number $N$ will be updated, as well as its corresponding PRRFF sinusoidal signal.

In the abovementioned PRRFF sinusoidal signal generation process, the pseudorandom number $N$ is mainly provided by the 32-bit xorshift random algorithm [38]

$$\begin{cases} X = (S_{j-1} \ll 13) \oplus S_{j-1} \\ Y = (X \gg 17) \oplus X \\ S_j = (Y \ll 5) \oplus Y \end{cases} \tag{7}$$

where the subscript "$j$" denotes the $j$th injection cycle, $\oplus$ denotes the bitwise XOR operator, $S_j$ is the 32-bit pseudorandom number among $[1, 2^{32}-1]$ with initial value 2463534242, and $X$ and $Y$ are the 32-bit intermediate variables. Then, the pseudorandom number $N$ with the value of 0 or 1 can be generated according to $S_j$ as

$$N = \begin{cases} 0, & S_j < P \cdot \left(2^{32}-1\right) \\ 1, & S_j \geq P \cdot \left(2^{32}-1\right) \end{cases} \tag{8}$$

where $P$ is the reversing probability of the sinusoidal signal, which is set as 0.5 in this article.

## B. Signal Injection and Electric Power Response

According to [18], to implement a signal-injection-based MTPA control, the HF signals injected into the $d$- and $q$-axis currents can be given as follows:

$$\begin{cases} i_{dh} = -i_{q0} A \sin\omega_h t \\ i_{qh} = i_{d0} A \sin\omega_h t \end{cases} \tag{9}$$

where $i_{d0}$ and $i_{q0}$ represent the dc components of the $d$- and $q$-axis currents, respectively. In the proposed method, the sign of the injection gain $A$ is pseudorandomly reversed. With the injected signals shown in (9), the $d$- and $q$-axis currents can be expressed as

$$\begin{cases} i_d = i_{d0} - i_{q0} A \sin\omega_h t \\ i_q = i_{q0} + i_{d0} A \sin\omega_h t \end{cases}. \tag{10}$$

The electric power $P_e$ is closely related to the $d$- and $q$-axis currents, which is usually expressed as (11) and can be further rewritten as (12) based on (1)–(3), where $\omega_m$ is the mechanical angular speed

$$P_e = \frac{3}{2}(u_d i_d + u_q i_q) \tag{11}$$

$$P_e = \frac{3}{2}\left[R\left(i_d^2 + i_q^2\right) + L_d i_d \frac{di_d}{dt} + L_q i_q \frac{di_q}{dt}\right] + \omega_m T_e(i_d, i_q). \tag{12}$$

Then, by substituting (10) into (12), the electric power response due to the signal injection can be derived as

$$\begin{aligned} P_e = {} & \tfrac{3}{2}R\left(i_{d0}^2 + i_{q0}^2\right)\left(1 + \tfrac{1}{2}A^2\right) \\ & - \tfrac{3}{4}R\left(i_{d0}^2 + i_{q0}^2\right)A^2 \cos 2\omega_h t \\ & + \tfrac{3}{4}\left(L_d i_{q0}^2 + L_q i_{d0}^2\right)\omega_h A^2 \sin 2\omega_h t \\ & - \tfrac{3}{2}\left(L_d - L_q\right) i_{d0} i_{q0} \omega_h A \cos\omega_h t + \omega_m T_e\left(i_d, i_q\right). \end{aligned} \tag{13}$$

It follows from (13) that to learn more detailed information contained in the resultant electric power response, the specific information about the resultant torque $T_e(i_d, i_q)$ is required. Based on the bivariate Taylor series expansion, the resultant torque $T_e(i_d, i_q)$ can be derived as

$$\begin{aligned} & T_e(i_d, i_q) \\ & = T_e(i_{d0} - i_{q0} A \sin\omega_h t, i_{q0} + i_{d0} A \sin\omega_h t) \\ & = T_e(i_{d0}, i_{q0}) + \left[i_{d0}\frac{\partial T_e}{\partial i_q}(i_{d0}, i_{q0}) - i_{q0}\frac{\partial T_e}{\partial i_d}(i_{d0}, i_{q0})\right] \end{aligned}$$

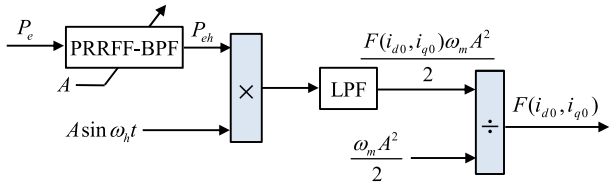


Fig. 3. Signal demodulation for extracting the MTPA indicator information $F(i_{d0},i_{q0})$.

$$A\sin\omega_h t+\cdots. \tag{14}$$

According to (6), the terms in the square brackets in (14), in effect, represents the dc component of the MTPA indicator $F$, i.e.,

$$F\left(i_{d0},i_{q0}\right)=i_{d0}\frac{\partial T_e}{\partial i_q}\left(i_{d0},i_{q0}\right)-i_{q0}\frac{\partial T_e}{\partial i_d}\left(i_{d0},i_{q0}\right). \tag{15}$$

Then, the resultant torque $T_e(i_d,\ i_q)$ shown in (14) can be rewritten as

$$T_e\left(i_d,i_q\right)=T_e\left(i_{d0},i_{q0}\right)+F\left(i_{d0},i_{q0}\right)A\sin\omega_h t+\cdots. \tag{16}$$

After the resultant torque $T_e(i_d,\ i_q)$ is derived, substituting (16) into (13) yields the detailed electric power response due to the signal injection, i.e.,

$$\begin{aligned}P_e=&\tfrac{3}{2}R\left(i_{d0}^2+i_{q0}^2\right)\left(1+\tfrac{1}{2}A^2\right)+\omega_m T_e\left(i_{d0},i_{q0}\right)\\&-\tfrac{3}{4}R\left(i_{d0}^2+i_{q0}^2\right)A^2\cos 2\omega_h t\\&+\tfrac{3}{4}\left(L_d i_{q0}^2+L_q i_{d0}^2\right)\omega_h A^2\sin 2\omega_h t\\&-\tfrac{3}{2}\left(L_d-L_q\right)i_{d0}i_{q0}\omega_h A\cos\omega_h t\\&+F\left(i_{d0},i_{q0}\right)\omega_m A\sin\omega_h t+\cdots.\end{aligned} \tag{17}$$

### C. Extraction of MTPA Indicator Information $F(i_{d0},\ i_{q0})$

Since the dc component of the MTPA indicator, i.e., $F(i_{d0},\ i_{q0})$ reflects that whether the operating point $(i_{d0},\ i_{q0})$ is the MTPA point, it is necessary to evaluate it. It follows from (17) that the MTPA indicator information $F(i_{d0},i_{q0})$ is contained in the $\sin\omega_h t$ component of the electric power $P_e$, and could be extracted through the signal demodulation shown in Fig. 3. As can be seen in Fig. 3, the electric power $P_e$ is first fed into a PRRFF band-pass filter (PRRFF-BPF) whose center frequency is $\omega_h$ (this BPF will be discussed in Section III-D), and only the pseudorandomly reversed injection frequency components (i.e., the terms being proportional to $A\sin\omega_h t$ and $A\cos\omega_h t$ in (17)) can be obtained. The output of the PRRFF-BPF, i.e., $P_{eh}$ is then multiplied by $A\sin\omega_h t$, and the product can be expressed as (18). This product is further filtered by a low-pass filter to obtain its dc component $F(i_{d0},\ i_{q0})\omega_m A^2/2$. Finally, the obtained dc component is divided by $\omega_m A^2/2$, extracting the MTPA indicator information $F(i_{d0},\ i_{q0})$

$$\begin{aligned}&\left[F(i_{d0},i_{q0})\omega_m A\sin\omega_h t\right.\\&\left.-\frac{3}{2}\left(L_d-L_q\right)i_{d0}i_{q0}\omega_h A\cos\omega_h t\right]\cdot A\sin\omega_h t\\&=-\frac{3(L_d-L_q)i_{d0}i_{q0}\omega_h A^2}{4}\sin 2\omega_h t\\&\quad-\frac{F(i_{d0},i_{q0})\omega_m A^2}{2}\cos 2\omega_h t+\frac{F(i_{d0},i_{q0})\omega_m A^2}{2}.\end{aligned} \tag{18}$$

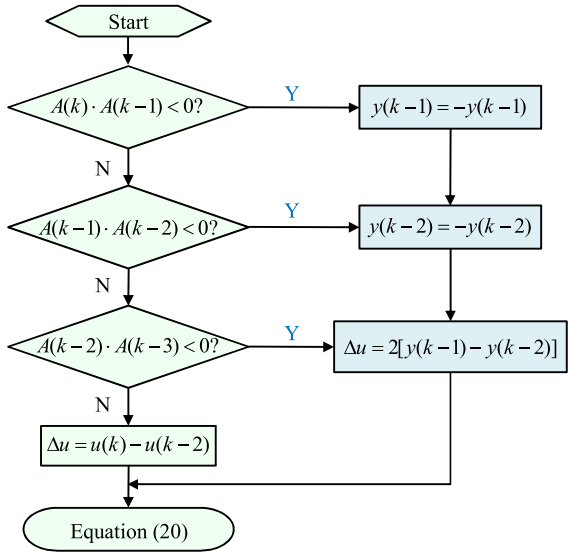


Fig. 4. Block diagram of the investigated PRRFF-BPF.

The extracted MTPA indicator information $F(i_{d0},\ i_{q0})$ will be employed to adjust the operating point of the motor until $F(i_{d0},\ i_{q0})=0$ is reached, i.e., the operating point locates on the MTPA point.

### D. PRRFF-BPF and Current Control Loop Considering PRRFF Signal Injection

The BPF is crucial for MTPA indicator extraction process, as shown in Fig. 3. In [37], the second-order BPF shown in (19) is adopted, where $\xi$ $(0<\xi<0.2)$ is the damping ratio

$$G_{\mathrm{BPF}}(s)=\frac{2\xi\omega_h s}{s^2+2\xi\omega_h s+\omega_h^2}. \tag{19}$$

With the Tustin method with frequency prewarping, the continuous-time transfer function (19) can be discretized as

$$y(k)=g_0\Delta u+g_1 y(k-1)+g_2 y(k-2) \tag{20}$$

where $g_{0,1,2}$ denote the gain constants, $k$ denotes the $k$th sampling period, $y(\cdot)$ denotes the output of the BPF, and

$$\Delta u=u(k)-u(k-2) \tag{21}$$

where $u(\cdot)$ denotes the input of the BPF.

In this article, the PRRFF sinusoidal signal is selected as the injection signal, and the above BPF cannot process such signal. To deal with this problem, a PRRFF-BPF is investigated in this article, as shown in Fig. 4. Since the PRRFF sinusoidal signal $A\sin\omega_h t$ is uniform sinusoidal signal within every segment that has the same sign of injection gain $A$, the PRRFF-BPF basically retains the form of the conventional BPF (20). Furthermore, considering that the PRRFF sinusoidal signal is obtained by

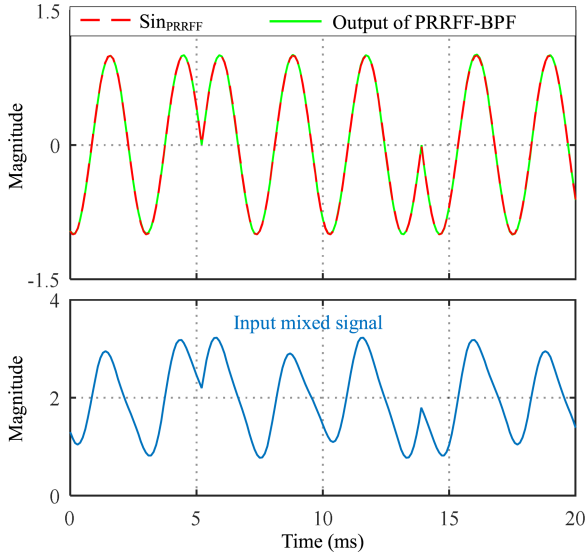


Fig. 5. Simulation results of the investigated PRRFF-BPF.

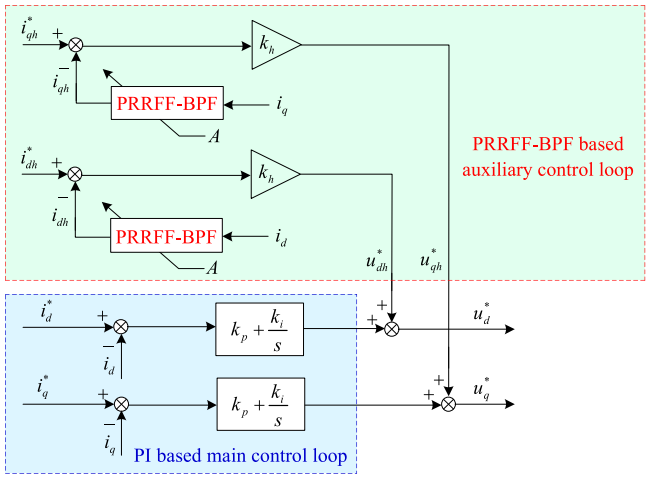


Fig. 6. Current control loop considering PRRFF signal injection.

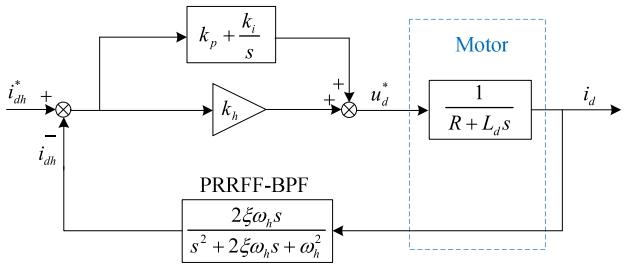


Fig. 7. Equivalent block diagram of the PRRFF current control loop.

piecewise reversing the conventional uniform sinusoidal signal, the PRRFF-BPF reassigns the input and output variables of the conventional BPF (20) using the history information, within three sampling periods after the sign of injection gain $A$ is changed. Specifically, when $A(k)\cdot A(k-1) < 0$, let $y(k-1) = -y(k-1)$; when $A(k-1)\cdot A(k-2)<0$, let $y(k-2) = -y(k-2)$; when $A(k-2)\cdot A(k-3) <0$, let $\Delta u = 2[y(k-1)-y(k-2)]$.

To verify the feasibility of the presented PRRFF-BPF, simulation was performed, and the results are shown in Fig. 5. In the simulation, the input mixed signal to be filtered is

$$f(t) = \mathrm{Sin}_{\mathrm{PRRFF}}(t) + 0.2\sin 2\omega_h t + 0.2\cos 0.5\omega_h t + 2 \quad (22)$$

where $\mathrm{Sin}_{\mathrm{PRRFF}}(t)$ denotes the unit PRRFF sinusoidal signal, i.e., $\mathrm{Sin}_{\mathrm{PRRFF}}(t) = (A/|A|)\sin\omega_h t$. It can be seen from Fig. 5 that the output of the PRRFF-BPF agrees well with the unit PRRFF sinusoidal signal $\mathrm{Sin}_{\mathrm{PRRFF}}(t)$, i.e., the PRRFF-BPF can well extract the PRRFF sinusoidal signal from the input mixed signal.

Given the satisfactory filtering performance of the presented PRRFF-BPF, it is employed to constitute a current control loop considering the required PRRFF signal injection in this article, as shown in Fig. 6.

As shown in Fig. 6, the current control loop consists of the PI based main control loop and the PRRFF-BPF based auxiliary control loop, which are mainly responsible for the closed-loop regulations for the dc components and the injected PRRFF components of the currents, respectively. In the PRRFF-BPF based auxiliary control loop, the references are the injected PRRFF signal references $i^*_{dh}$ and $i^*_{qh}$, and the feedbacks are the PRRFF current components (i.e., $i_{dh}$ and $i_{qh}$) obtained by filtering the $d$- and $q$-axis currents with PRRFF-BPFs. In this way, the auxiliary control loop can only regulate the PRRFF components without influencing the dc components.

The controller parameter $k_h$ in the auxiliary control loop is crucial for the PRRFF current components tracking. If an inappropriate value is selected, the PRRFF current components tracking error may be occurred. This may influence the MTPA control accuracy, as derived in Appendix A. Hence, the controller parameter $k_h$ needs to be designed carefully.

Given that the PI based main control loop has certain effect on the regulation of the injected components [37], the equivalent block diagram of the PRRFF current control loop (take the $d$-axis as an example) can be shown in Fig. 7. Since the PRRFF-BPF is the same as the conventional BPF within every segment having the same sign of injection gain $A$, (19) can be served as the transfer function of the PRRFF-BPF in the controller parameter design, as shown in Fig. 7.

From Fig. 7, the transfer function of the equivalent PRRFF current control loop can be derived as (23) shown at the bottom of this page.

Substituting $s = j\omega_h$ into (23), the frequency characteristic of (23) at the injection frequency $\omega_h$ can be obtained as

$$\frac{i_{dh}(j\omega_h)}{i^*_{dh}(j\omega_h)} = \frac{k_i + j\omega_h(k_h + k_p)}{k_i - \omega_h^2 L_d + j[\omega_h(k_h + k_p) + \omega_h R]}. \quad (24)$$

$$\frac{i_{dh}(s)}{i^*_{dh}(s)} = \frac{2\xi\omega_h(k_h + k_p)s + 2\xi\omega_h k_i}{L_d s^3 + (2\xi\omega_h L_d + R)s^2 + [\omega_h^2 L_d + 2\xi\omega_h(k_h + k_p) + 2\xi\omega_h R]s + \omega_h^2 R + 2\xi\omega_h k_i} \quad (23)$$

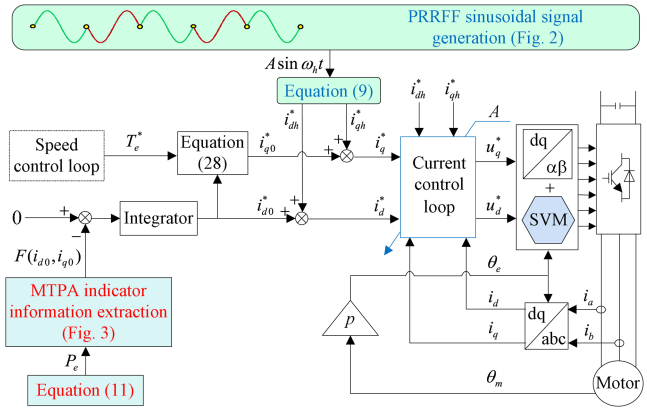


Fig. 8. Block diagram of the proposed MTPA control strategy based on PRRFF sinusoidal signal generation.

It follows from (24) that if the condition (25) is satisfied, (26) can be obtained

$$\begin{cases} \omega_h(k_h+k_p) \gg k_i \\ \omega_h(k_h+k_p) \gg \left|(k_i-\omega_h^2 L_d)+j\omega_h R\right| \end{cases} \tag{25}$$

$$\frac{i_{dh}(j\omega_h)}{i_{dh}^*(j\omega_h)} \approx 1. \tag{26}$$

Equation (26) shows that at the injection frequency, the PRRFF current reference $i_{dh}^*$ can be accurately tracked by $i_{dh}$. Similarly, the PRRFF current reference $i_{qh}^*$ can also be accurately tracked by $i_{qh}$. This means that the overall current control loop shown in Fig. 6 can achieve an accurate PRRFF current component tracking, which can satisfy the current injection requirement of the proposed MTPA control method. The validation of the PRRFF current component tracking performance of this current control loop will be given in Section IV.

The abovementioned discussions show that the key to realizing an accurate PRRFF current component tracking is making (25) true. This means that the proportional gain $k_h$ in the auxiliary current control loop should meet

$$\begin{cases} k_h >> (k_i-\omega_h k_p)/\omega_h \\ k_h >> -\left(\omega_h k_p - \sqrt{(k_i-\omega_h^2 L_d)^2+\omega_h^2 R^2}\right)\Big/\omega_h \end{cases}. \tag{27}$$

### E. Implementation of the Proposed MTPA Control Method

Based on the abovementioned discussions, the proposed MTPA control approach can be implemented, as depicted in Fig. 8. The PRRFF sinusoidal signal generation module is responsible for providing the desired PRRFF sinusoidal signal, and the injected signal references $i_{dh}^*$ and $i_{qh}^*$ can be generated based on (9) accordingly. Then, with the current control loop, the injected signals can be injected into the $d$- and $q$-axis currents in accordance with their references $i_{dh}^*$ and $i_{qh}^*$. In such a case, it follows from Sections III–B and III–C that the MTPA indicator information $F(i_{d0}, i_{q0})$ can be extracted from the electric power $P_e$ through the signal demodulation shown in Fig. 3. Considering that $F(i_{d0}, i_{q0})$ is equal to zero at the MTPA point, a closed-loop control of $F(i_{d0}, i_{q0})$ with zero given value is constructed in the proposed method, and the output of the regulator (i.e., integrator) is employed to adjust the reference of $i_{d0}$ (i.e., $i_{d0}^*$). With the help of this closed-loop control, $F(i_{d0}, i_{q0})$ can be controlled to zero, and the operating points $(i_{d0}, i_{q0})$ will be located on the MTPA points accordingly, thus achieving an accurate MTPA control.

In the proposed method, the reference of $i_{q0}$ (i.e., $i_{q0}^*$) is generated according to (28), and the involved motor parameters are assigned their nominal values. Since the generation of the reference $i_{d0}^*$ is independent of $i_{q0}^*$, to calculate $i_{q0}^*$ with inaccurate motor parameters will not affect the accuracy of MTPA point tracking [11]. The adoption of inaccurate motor parameters in (28) may result in torque error, which can be automatically compensated by a speed control loop

$$i_{q^0}^* = \frac{T_e^*}{\frac{3}{2}p[\Psi_f+(L_d-L_q)]i_{d^0}^*}. \tag{28}$$

Unlike the conventional fixed-frequency signal injection methods, the proposed method uses nonrepetitive (i.e., PRRFF) sinusoidal signals as the injected signals. In this way, the induced HF components in motor currents are no longer concentrated at certain frequencies, and hence, the proposed method can realize lower injection-induced CSPs compared with the conventional methods. Moreover, different from the pseudorandom-frequency injection method, the proposed method employs the fixed injection frequency, and hence, avoids the difficulty of matching candidate injection frequencies.

TABLE I
SPECIFICATION OF THE IPMSM

| | | | |
|---|---|---|---|
| Rated power | 4 kW | Number of pole pairs | 4 |
| Rated torque | 38 N·m | Stator resistance | 0.08 Ω |
| Rated speed | 1000 r/min | PM flux linkage | 0.14 Wb |
| Rated current | 40 A | $d$-$q$ axis inductances | 2.3/3.8 mH |

## IV. Simulation and Experimental Results

### A. Simulation Results

To verify the control performance of the proposed method, simulations were conducted in MATLAB/Simulink. The IPMSM model is parameter-variable, and its nominal parameters are given in Table I. In the simulations, the injection frequency is 344.83 Hz, and the injection gain $A = \pm 0.05$.

Simulations were first performed at 1000 r/min under a set of step torque levels within 10 to 50 N·m, and the results are presented in Fig. 9. As can be seen, the $d$- and $q$-axis currents are tightly centered around the dc current references $i_{d0}^*$ and $i_{q0}^*$. This means that the investigated current control loop (see Fig. 6) can realize satisfactory dc current tracking performance under PRRFF signal injection. Also, it can be seen that the dc components of the $d$- and $q$-axis currents matches well with the real MTPA points under different torque levels. This means that a high MTPA control accuracy can be achieved with the proposed method.

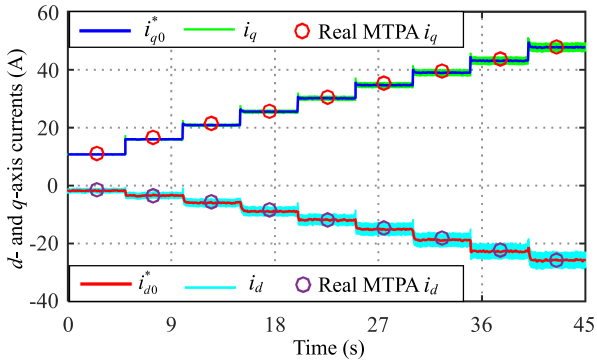


Fig. 9. Simulation results of the proposed method at 1000 r/min under a set of step torque levels within 10 to 50 N·m.

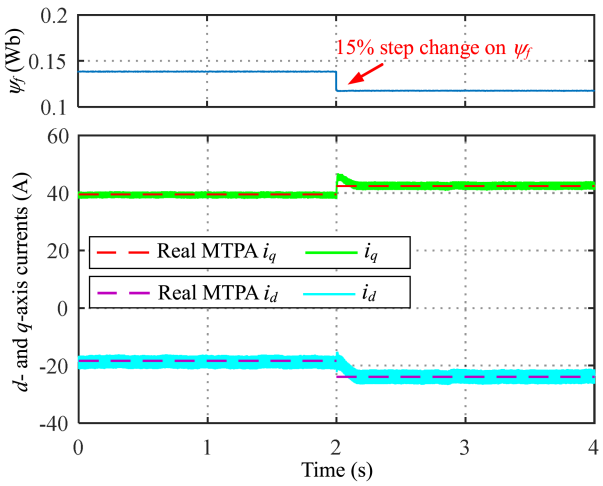


Fig. 10. Simulation results of the proposed method under 40 N·m when temperature changes.

Given that the permanent magnet (PM) flux linkage may vary with temperature, the influence of the temperature rise on MTPA control accuracy was investigated by changing the PM flux linkage. The motor was operated in speed control mode at 1000 r/min under 40 N·m, and the PM flux linkage was abruptly reduced to 85% of its original value at $t = 2$ s. The results are shown in Fig. 10, where it can be seen that although the actual MTPA currents were changed (at $t = 2$ s) due to the change of the PM flux linkage, the proposed method can finally and accurately track the new MTPA currents. Therefore, the proposed method is robust to temperature rise.

Simulations were also performed under step speed references and step load torque. Specifically, the step speed references are 400-1000-400 r/min, and the results are shown in Fig. 11; the step load torque is 10-40-10 N·m, and the results are shown in Fig. 12. The results in Figs. 11 and 12 show that the proposed method is robust to the severe operating conditions.

## B. Experimental Results

The performance of the proposed method was evaluated based on the experimental setup shown in Fig. 13, where the tested IPMSM is operated in torque control mode and the dynamometer

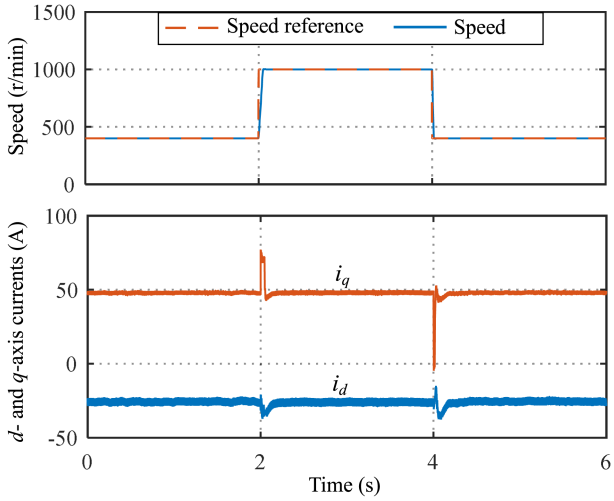


Fig. 11. Simulation results of the proposed method under 50 N·m when step speed reference changes according to 400-1000-400 r/min.

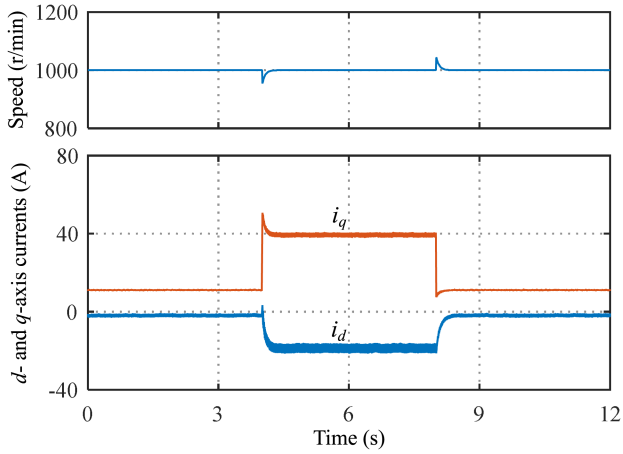


Fig. 12. Simulation results of the proposed method at 1000 r/min under step load torque 10-40-10 N·m.

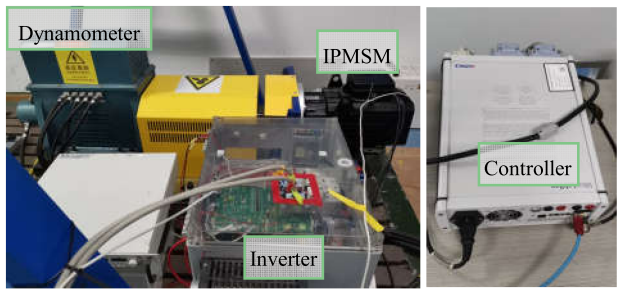


Fig. 13. Experimental setup.

coaxially connected to the IPMSM is operated in speed control mode. The parameters of the tested IPMSM are listed in Table I. The control algorithm is executed through dSPACE DS1202. In this algorithm, the pulsewidth modulation (PWM) frequency and the sampling frequency are both 10 kHz, the pseudorandom number $N$ is updated every 3 sinusoidal cycles, the injection frequency is 344.83 Hz, and the injection gain $A = \pm 0.05$. Given

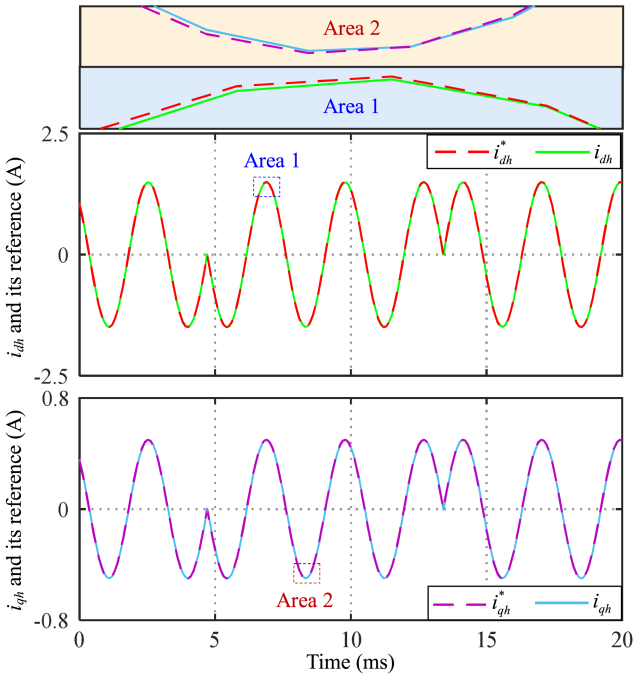


Fig. 14. Experimental results of the PRRFF sinusoidal signal tracking of the current control loop.

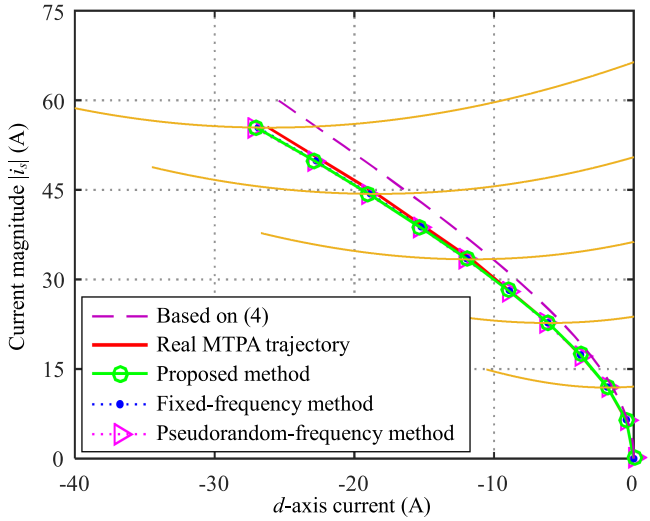


Fig. 15. Experimental current trajectories of the proposed method and the comparable methods.

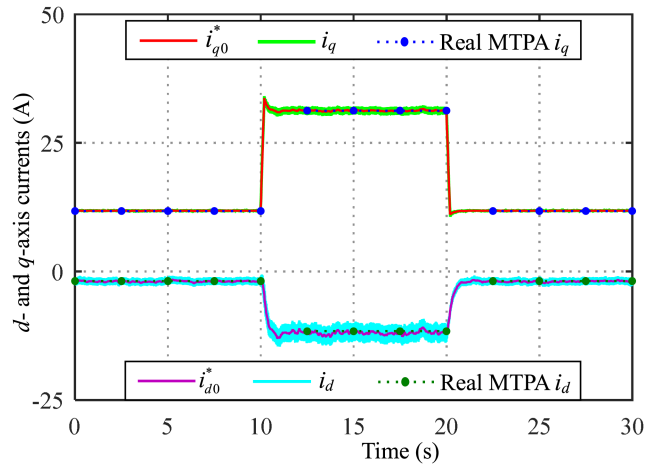


Fig. 16. Experimental results of the proposed method at 500 r/min during an abrupt torque of 10-30-10 N·m.

that the actual gain of the BPFs slightly varies with discretization way (including frequency prewarping), for fair comparison, the BPFs in the proposed and the comparable schemes are discretized in the same way, i.e., Tustin method with frequency prewarping.

The PRRFF sinusoidal signal tracking performance of the current control loop (see Fig. 6) was first examined, and the results are shown in Fig. 14. In the experiment, the magnitudes of the PRRFF sinusoidal current references $i_{dh}^*$ and $i_{qh}^*$ are manually set as 1.5 and 0.5 A, respectively. The results show that the feedback PRRFF sinusoidal currents $i_{dh}$ and $i_{qh}$ track their corresponding references $i_{dh}^*$ and $i_{qh}^*$ accurately. Hence, the current control loop can well meet the PRRFF sinusoidal current injection requirement of the proposed method.

To verify the MTPA control accuracy of the presented method, tests under different torque levels were carried out. The current trajectory connected by the obtained steady-state operating points is plotted in the $|i_s|$-$i_d$ plane, as shown in Fig. 15. For observation and comparison purposes, the real MTPA current trajectory, the current trajectory based on (4) using constant parameters, and the constant torque curves (of 10, 20, 30, 40, and 50 N·m) are also shown in Fig. 15. It can be seen that the current trajectory based on (4) noticeably deviates from the real MTPA current trajectory. This is because the motor parameter variations are neglected. In contrast, the current trajectory of the proposed method agrees well with the real MTPA current trajectory. In other words, the proposed method can realize a high MTPA control accuracy. Also, it can be seen that the current trajectory of the proposed method matches well with that of the fixed-frequency injection method and the pseudorandom-frequency injection method [37]. This means that the adoption of the PRRFF injection signals in the proposed method does not degrade the MTPA control accuracy.

In addition to steady-state conditions, the proposed method was also tested under dynamic conditions. Fig. 16 shows the $d$- and $q$-axis current responses at 500 r/min during an abrupt torque of 10-30-10 N·m. As can be seen, the dc components of the $d$- and $q$-axis currents track the dc current references ($i_{d0}^*$ and $i_{q0}^*$) and the real MTPA currents quickly and accurately, after the torque changes abruptly. This demonstrates that the proposed method is robust to torque transients and exhibits satisfactory dynamic performance.

To evaluate the performance of the proposed method in terms of injection-induced CSP reduction, the proposed PRRFF method and the conventional fixed-frequency method were contrastively tested at 600 r/min under 40 N·m with the same injection frequency. Fig. 17 shows the resultant motor phase currents and their fast Fourier transform (FFT) results. It can be seen that the phase current FFT result of the conventional

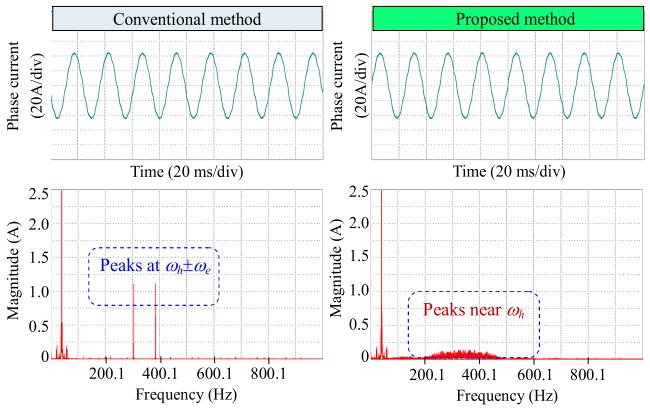


Fig. 17. Motor phase currents and their FFT results of both the proposed method and the conventional fixed-frequency method at 600 r/min under 40 N·m.

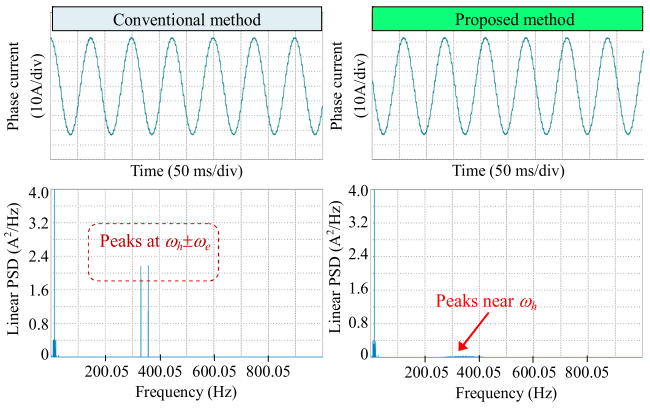


Fig. 19. Motor phase currents and their PSD results of both the proposed method and the conventional fixed-frequency method at 200 r/min under 30 N·m.

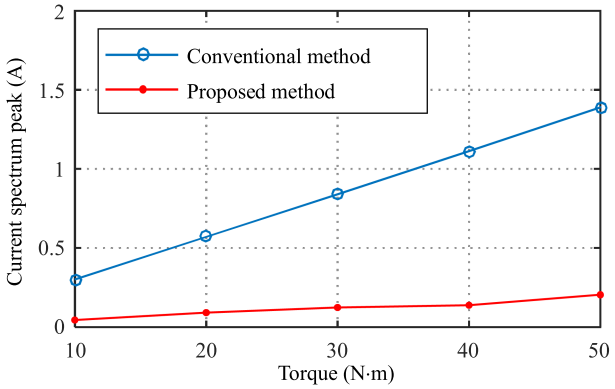


Fig. 18. Injection-induced maximum CSPs of the conventional fixed-frequency method and the proposed method under different torque levels.

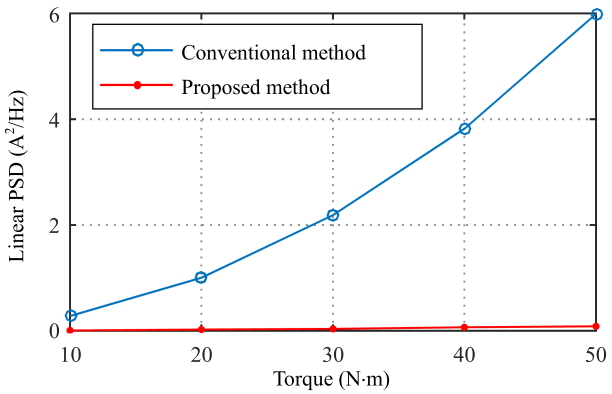


Fig. 20. Injection-induced maximum current PSD peaks of the conventional fixed-frequency method and the proposed method under different torque levels.

fixed-frequency method exhibits two high discrete peaks at frequencies of $\omega_h \pm \omega_e$, which are induced by the uniform sinusoidal signals injected into the $d$- and $q$-axis currents. In striking contrast to the conventional method, the phase current FFT result of the proposed method shows very low peaks near the frequency of $\omega_h$. In other words, the injection-induced CSPs of the presented method are far lower than that of the conventional method.

For intuitive comparison, Fig. 18 summarizes the injection-induced maximum CSPs of the conventional fixed-frequency method and the presented method under different torque levels. The results show that compared with the conventional method, the proposed method can achieve significantly lower injection-induced CSPs, regardless of torque levels. This benefits from the pseudorandom characteristic of the injected PRRFF signals. The theoretical analysis about why the proposed method can reduce the injection-induced CSPs is conducted in Appendix B.

For stationary random signals, power spectral density (PSD) is a frequently-used tool to analyze the frequency-domain characteristic [39]. Hence, the motor phase current of the proposed method obtained under 30 N·m at 200 r/min was analyzed with this tool, and the analysis result is shown in Fig. 19. For comparison, the current PSD analysis result of the conventional method is also given in Fig. 19. It should be noted that the PSD results in Fig. 19 are in linear form. It can be seen that the phase current PSD of the conventional method contains two discrete spectra at frequencies of $\omega_h \pm \omega_e$, whereas that of the proposed method contains some continuous spectra near the frequency of $\omega_h$, and the phase current PSD peaks of the proposed method are far lower than that of the conventional method. This implies that the proposed method can approximately extend the injection-induced electromagnetic noise to the white noise within a limited bandwidth, thus reducing the possible negative effects caused by the injected signals.

Fig. 20 compares the injection-induced maximum current PSD peaks of the conventional method with that of the presented method under different torque levels. It can be observed that, for any given torque level, the presented method can realize a far lower injection-induced current PSD peak than that of the conventional method. Hence, the characteristic that the presented method has remarkable CSP reduction effect is also validated from the PSD point of view.

## V. Discussions

In the proposed method, the injection frequency $\omega_h$ needs to be selected, and whose selection should follow the following principles.

1) One injection period ($2\pi/\omega_h$) should be integral multiples of the sampling period, to make the PRRFF sinusoidal signal reverse at zero crossing points.
2) To guarantee the PRRFF current injection performance, one injection period should be at least 20 times the sampling period.
3) To guarantee the MTPA dynamic tracking performance, the injection frequency should be at least 100 Hz.
4) For low PWM frequency applications, to make the injection frequency meet the requirements of 2) and 3), the dual-sampling-dual-update technique can be employed, i.e., the signal sampling and duty update are conducted twice during each PWM period.

In addition to the injection frequency $\omega_h$, the injection gain $A$ also needs to be selected. The larger the injection gain, the higher the injection SNR; the smaller the injection gain, the smaller the negative effects caused by injection. In this case, the selection of the injection gain should follow the principle that selecting the minimum value that satisfies the required injection SNR. Based on this principle, the injection gain $A$ can be easily selected within the range $0.02 \leq A \leq 0.08$ through simple offline tests.

## VI. Conclusion

This article presented an MTPA control method based on PRRFF sinusoidal signal injection for IPMSM drives, which can realize an MTPA control with satisfactory performance. To facilitate this method, a PRRFF-BPF was investigated and then utilized to construct a current control loop considering the PRRFF signal injection. Unlike the conventional fixed-frequency injection methods, the proposed method adopts the nonrepetitive (i.e., PRRFF) sinusoidal signal as the injected signals, allowing the injection-induced CSPs to be significantly reduced. In addition, unlike the pseudorandom-frequency injection method, the proposed method employs the fixed injection frequency, avoiding the difficult matching of candidate injection frequencies. The performance of the proposed scheme has been verified on a prototype IPMSM drive system.

## Appendix A

If a large PRRFF current components tracking error is existed. Taking the $d$-axis as an example, the injected $d$- and $q$-axis current components shown in (9) become

$$\begin{cases} i_{dh} = -i_{q0} A\eta \sin \omega_h t \\ i_{qh} = i_{d0} A \sin \omega_h t \end{cases} \tag{A1}$$

where $\eta$ ($0 < \eta < 1$) represents the effect of the injection error. It follows from the derivation process from (9) to (17) that the electric power response due to the injected signals (A1) can be expressed as

$$\begin{aligned} P_e = {} & P_0 + P_{\cos} + P_{\sin 2} + P_{\cos 2} \\ & + \left[F(i_{d0}, i_{q0})\omega_m + 3(1-\eta)Ri_{d0}i_{q0} \right. \\ & \left. + (1-\eta)i_{q0}\omega_m \frac{\partial T_e}{\partial i_d}(i_{d0}, i_{q0})\right] A \sin \omega_h t \end{aligned} \tag{A2}$$

where $P_0$, $P_{\cos}$, $P_{\sin 2}$, $P_{\cos 2}$ represent the dc component, $\cos\omega_h t$ component, $\sin 2\omega_h t$ component, and $\cos 2\omega_h t$ component of the electric power $P_e$, respectively. Then, by means of the signal demodulation shown in Fig. 3, it can be deduced that the extracted information from the electric power $P_e$ can be expressed as

$$\begin{aligned} P_{dem} = {} & F(i_{d0}, i_{q0}) + \frac{3(1-\eta)Ri_{d0}i_{q0}}{\omega_m} \\ & + (1-\eta)i_{q0}\frac{\partial T_e}{\partial i_d}(i_{d0}, i_{q0}). \end{aligned} \tag{A3}$$

This implies that in the case of the injected signals (A1), the information extracted from the electric power $P_e$ is no longer the exact MTPA indicator $F(i_{d0}, i_{q0})$. Hence, the MTPA control accuracy may be influenced.

## Appendix B

According to (10), the motor phase current after signal injection can be expressed as

$$\begin{aligned} i_a(t) = {} & i_{d0}\cos\omega_e t - i_{q0}\sin\omega_e t - 0.5i_{q0}A\sin(\omega_h + \omega_e)t \\ & + 0.5i_{d0}A\cos(\omega_h + \omega_e)t - 0.5i_{q0}A\sin(\omega_h - \omega_e)t \\ & - 0.5i_{d0}A\cos(\omega_h - \omega_e)t. \end{aligned} \tag{A4}$$

From (A4), the HF components of the phase current can be expressed as

$$\begin{aligned} i_{ah}(t) = {} & -0.5i_{q0}A\sin(\omega_h + \omega_e)t + 0.5i_{d0}A\cos(\omega_h + \omega_e)t \\ & - 0.5i_{q0}A\sin(\omega_h - \omega_e)t - 0.5i_{d0}A\cos(\omega_h - \omega_e)t. \end{aligned} \tag{A5}$$

Based on Parseval's theorem, during a certain time $T_x$, the following relationship is true [28], i.e.,:

$$\int_0^{T_x} \left[i_{ah}(t)\right]^2 dt = \int_{-\infty}^{+\infty} \left[I_{ah}(\omega_f)\right]^2 d\omega_f \tag{A6}$$

where $I_{ah}(\omega_f)$ is the Fourier transform of the HF phase current $i_{ah}(t)$. As shown on the left side of (A6), the HF phase current under the conventional injection and that under the PRRFF injection have nearly the same energy. According to (A5), $I_{ah}(\omega_f)$ under conventional injection is concentrated at two discrete frequencies $\omega_h \pm \omega_e$, while $I_{ah}(\omega_f)$ under the PRRFF injection is distributed at a wide frequency range due to the pseudorandomly reversed injection gain $A$. Then, it follows from (A6) that under the PRRFF injection, the injection-induced CSPs can be reduced.

## References

[1] Y. Zhang, Z. Yin, F. Gao, and J. Liu, "Research on anti-DC bias and high-order harmonics of a fifth-order flux observer for IPMSM sensorless drive," *IEEE Trans. Ind. Electron.*, vol. 69, no. 4, pp. 3393–3406, Apr. 2022.
[2] F. J. Lin, Y. T. Liu, and W. A. Yu, "Power perturbation based MTPA with an online tuning speed controller for an IPMSM drive system," *IEEE Trans. Ind. Electron.*, vol. 65, no. 5, pp. 3677–3687, May 2018.
[3] A. Dianov, F. Tinazzi, S. Calligaro, and S. Bolognani, "Review and classification of MTPA control algorithms for synchronous motors," *IEEE Trans. Power Electron.*, vol. 37, no. 4, pp. 3990–4007, Apr. 2022.

[4] A. Shinohara, Y. Inoue, S. Morimoto, and M. Sanada, "Direct calculation method of reference flux linkage for maximum torque per ampere control in DTC-based IPMSM drives," *IEEE Trans. Power Electron.*, vol. 32, no. 3, pp. 2114–2122, Mar. 2017.
[5] Z. Xia, S. Nalakath, R. Tarvirdilu Asl, Y. Sun, J. Wiseman, and A. Emadi, "Online optimal tracking method for interior permanent magnet machines with improved MTPA and MTPV in whole speed and torque ranges," *IEEE Trans. Power Electron.*, vol. 35, no. 9, pp. 9753–9769, Sep. 2020.
[6] G. Foo and M. F. Rahman, "Sensorless sliding-mode MTPA control of an IPM synchronous motor drive using a sliding-mode observer and HF signal injection," *IEEE Trans. Ind. Electron.*, vol. 57, no. 4, pp. 1270–1278, Apr. 2010.
[7] S. Y. Jung, J. Hong, and K. Nam, "Current minimizing torque control of the IPMSM using Ferrari's method," *IEEE Trans. Power Electron.*, vol. 28, no. 12, pp. 5603–5617, Dec. 2013.
[8] H. S. Kim, J. Yoo, and S. K. Sul, "Online MTPA operation of IPMSM based on dual-loop control in polar coordinates," *IEEE Trans. Power Electron.*, vol. 37, no. 4, pp. 4431–4441, Apr. 2022.
[9] Y. A. R. I. Mohamed and T. K. Lee, "Adaptive self-tuning MTPA vector controller for IPMSM drive system," *IEEE Trans. Energy Convers.*, vol. 21, no. 3, pp. 636–644, Sep. 2006.
[10] K. Li and Y. Wang, "Maximum torque per ampere (MTPA) control for IPMSM drives based on a variable-equivalent-parameter MTPA control law," *IEEE Trans. Power Electron.*, vol. 34, no. 7, pp. 7092–7102, Jul. 2019.
[11] T. Sun, M. Koc, and J. Wang, "MTPA control of IPMSM drives based on virtual signal injection considering machine parameter variations," *IEEE Trans. Ind. Electron.*, vol. 65, no. 8, pp. 6089–6098, Aug. 2018.
[12] G. Wang, Z. Li, G. Zhang, Y. Yu, and D. Xu, "Quadrature PLL-based high-order sliding-mode observer for IPMSM sensorless control with online MTPA control strategy," *IEEE Trans. Energy Convers.*, vol. 28, no. 1, pp. 214–224, Mar. 2013.
[13] S. Bolognani, R. Petrella, A. Prearo, and L. Sgarbossa, "Automatic tracking of MTPA trajectory in IPM motor drives based on AC current injection," *IEEE Trans. Ind. Appl.*, vol. 47, no. 1, pp. 105–114, Jan./Feb. 2011.
[14] C. Lai, G. Feng, K. Mukherjee, J. Tjong, and N. C. Kar, "Maximum torque per ampere control for IPMSM using gradient descent algorithm based on measured speed harmonics," *IEEE Trans. Ind. Inform.*, vol. 14, no. 4, pp. 1424–1435, Apr. 2018.
[15] R. Antonello, M. Carraro, and M. Zigliotto, "Maximum-torque-per-ampere operation of anisotropic synchronous permanent-magnet motors based on extremum seeking control," *IEEE Trans. Ind. Electron.*, vol. 61, no. 9, pp. 5086–5093, Sep. 2014.
[16] S. Kim, Y. D. Yoon, S. K. Sul, and K. Ide, "Maximum torque per ampere (MTPA) control of an IPM machine based on signal injection considering inductance saturation," *IEEE Trans. Power Electron.*, vol. 28, no. 1, pp. 488–497, Jan. 2013.
[17] G. Liu, J. Wang, W. Zhao, and Q. Chen, "A novel MTPA control strategy for IPMSM drives by space vector signal injection," *IEEE Trans. Ind. Electron.*, vol. 64, no. 12, pp. 9243–9252, Dec. 2017.
[18] K. Li and Y. Wang, "Maximum torque per ampere (MTPA) control for IPMSM drives using signal injection and an MTPA control law," *IEEE Trans. Ind. Inform.*, vol. 15, no. 10, pp. 5588–5598, Oct. 2019.
[19] G. Wang, H. Zhou, N. Zhao, C. Li, and D. Xu, "Sensorless control of IPMSM drives using a pseudo-random phase-switching fixed-frequency signal injection scheme," *IEEE Trans. Ind. Electron.*, vol. 65, no. 10, pp. 7660–7671, Oct. 2018.
[20] T. Sun, J. Wang, and X. Chen, "Maximum torque per ampere (MTPA) control for interior permanent magnet synchronous machine drives based on virtual signal injection," *IEEE Trans. Power Electron.*, vol. 30, no. 9, pp. 5036–5045, Sep. 2015.
[21] T. Sun, J. Wang, and M. Koc, "Self-learning direct flux vector control of interior permanent-magnet machine drives," *IEEE Trans. Power Electron.*, vol. 32, no. 6, pp. 4652–4662, Jun. 2017.
[22] Q. Tang, A. Shen, P. Luo, H. Shen, W. Li, and X. He, "IPMSMs sensorless MTPA control based on virtual q-axis inductance by using virtual high-frequency signal injection," *IEEE Trans. Ind. Electron.*, vol. 67, no. 1, pp. 136–146, Jan. 2020.
[23] Q. Chen, W. Zhao, G. Liu, and Z. Lin, "Extension of virtual-signal-injection-based MTPA control for five-phase IPMSM into fault-tolerant operation," *IEEE Trans. Ind. Electron.*, vol. 66, no. 2, pp. 944–955, Feb. 2019.
[24] J. Wang et al., "An accurate virtual signal injection control of MTPA for an IPMSM with fast dynamic response," *IEEE Trans. Power Electron.*, vol. 33, no. 9, pp. 7916–7926, Sep. 2018.
[25] Z. Han, J. Liu, W. Yang, D. B. Pinhal, N. Reiland, and D. Gerling, "Improved online maximum-torque-per-ampere algorithm for speed controlled interior permanent magnet synchronous machine," *IEEE Trans. Ind. Electron.*, vol. 67, no. 5, pp. 3398–3408, May 2020.
[26] T. Sun, L. Long, R. Yang, K. Li, and J. Liang, "Extended virtual signal injection control for MTPA operation of IPMSM drives with online derivative term estimation," *IEEE Trans. Power Electron.*, vol. 36, no. 9, pp. 10602–10611, Sep. 2021.
[27] G. Zhang, G. Wang, H. Wang, D. Xiao, L. Li, and D. Xu, "Pseudorandom-frequency sinusoidal injection based sensorless IPMSM drives with tolerance for system delays," *IEEE Trans. Power Electron.*, vol. 34, no. 4, pp. 3623–3632, Apr. 2019.
[28] B. Du, T. Zhao, S. Han, L. Song, and S. Cui, "Sensorless control strategy for IPMSM to reduce audible noise by variable frequency current injection," *IEEE Trans. Ind. Electron.*, vol. 67, no. 2, pp. 1149–1159, Feb. 2020.
[29] G. Wang, L. Yang, G. Zhang, X. Zhang, and D. Xu, "Comparative investigation of pseudorandom high-frequency signal injection schemes for sensorless IPMSM drives," *IEEE Trans. Power Electron.*, vol. 32, no. 3, pp. 2123–2132, Mar. 2017.
[30] Y. Zhang, Z. Yin, J. Liu, R. Zhang, and X. Sun, "IPMSM sensorless control using high-frequency voltage injection method with random switching frequency for audible noise improvement," *IEEE Trans. Ind. Electron.*, vol. 67, no. 7, pp. 6019–6030, Jul. 2020.
[31] Z. Yang, K. Wang, and X. Sun, "Novel random square-wave voltage injection method based on Markov chain for IPMSM sensorless control," *IEEE Trans. Power Electron.*, vol. 37, no. 11, pp. 13147–13157, Nov. 2022.
[32] S. Chen, W. Ding, X. Wu, R. Hu, and S. Shi, "Novel random high-frequency square-wave and pulse voltage injection scheme-based sensorless control of IPMSM drives," *IEEE J. Emerg. Sel. Topics Power Electron.*, vol. 11, no. 2, pp. 1705–1721, Apr. 2023.
[33] G. Bi, G. Wang, G. Zhang, N. Zhao, and D. Xu, "Low-noise initial position detection method for sensorless permanent magnet synchronous motor drives," *IEEE Trans. Power Electron.*, vol. 35, no. 12, pp. 13333–13344, Dec. 2020.
[34] C. Li, G. Wang, G. Zhang, N. Zhao, and D. Xu, "Adaptive pseudo-random high-frequency square-wave voltage injection based sensorless control for SynRM drives," *IEEE Trans. Power Electron.*, vol. 36, no. 3, pp. 3200–3210, Mar. 2021.
[35] Y. Zhang, Z. Yin, C. Du, J. Liu, and X. Sun, "Noise spectrum shaping of random high-frequency-voltage injection based on Markov chain for IPMSM sensorless control," *IEEE J. Emerg. Sel. Topics Power Electron.*, vol. 8, no. 4, pp. 3682–3699, Dec. 2020.
[36] J. Chen, Y. Fan, W. Wang, C. H. T. Lee, and Y. Wang, "Sensorless control for SynRM drives using a pseudo-random high-frequency triangular-wave current signal injection scheme," *IEEE Trans. Power Electron.*, vol. 37, no. 6, pp. 7122–7131, Jun. 2022.
[37] K. Li, T. Sun, F. Jiang, W. Feng, and H. Li, "MTPA control for IPMSM drives based on pseudorandom frequency-switching sinusoidal signal injection," *Machines*, vol. 10, no. 4, pp. 1–16, Apr. 2022.
[38] G. Marsaglia, "Xorshift RNGs," *J. Stat. Softw.*, vol. 8, no. 14, pp. 1–6, Jul. 2003.
[39] G. Zhang et al., "Hybrid pseudorandom signal injection for position sensorless SynRM drives with acoustic noise reduction," *IEEE Trans. Transport. Electrific.*, vol. 8, no. 1, pp. 1313–1325, Mar. 2022.

**Ke Li** was born in Shandong, China. He received the B.S. degree in electrical engineering from Shandong University of Technology, Zibo, China, in 2009, and the M.S. and Ph.D. degrees from Harbin Institute of Technology, Shenzhen, China, in 2011 and 2019, respectively, in electrical engineering.

Since 2020, he has been a Postdoctoral Fellow with the Shenzhen Institutes of Advanced Technology, Chinese Academy of Sciences, Shenzhen, China. His current research interests include MTPA control for PMSM drives and small dc-link capacitance motor drives.

**Tianfu Sun** (Senior Member, IEEE) was born in China. He received the B.Eng. degree in mechanical engineering, the M.Sc. degree in civil engineering (mechanics) from Dalian University of Technology, Dalian, China, in 2009 and 2012, respectively, and the Ph.D. degree in electrical and electronic engineering from the University of Sheffield, Sheffield, U.K., in 2016.

From 2016 to 2017, he was with the Department of Electronic and Electrical Engineering, University of Sheffield, Sheffield, U.K., where he was a Postdoctoral Research Fellow. He is currently an Associate Professor in electric drives with Shenzhen Institutes of Advanced Technology, Chinese Academy of Sciences, Shenzhen, China. His current research interests include machine design, power electronics, and motor drives.

Dr. Sun was selected as a member of Youth Innovation Promotion Association of Chinese Academy of Sciences.

**Jianing Liang** received the B.S. degree in electrical engineering and automation from Shenyang University of Technology, Shenyang, China, in 2003, and the M.S. degree in electrical and mechatronics engineering and the Ph.D. degree in industrial and systems engineering from Kyungsung University, Busan, South Korea, in 2007 and 2010, respectively.

He is currently an Associate Professor with the Shenzhen Institutes of Advanced Technology, Chinese Academy of Sciences, Shenzhen, China. His current research interests include advanced motor drive system and design of power converter.

**Mikail Koc** was born in Turkey. He received the B.Sc. degree in electrical and electronics engineering from Eskişehir Osmangazi University, Eskisehir, Turkey, in 2009, the M.Sc. degree in electrical and electronics engineering from Nottingham University, Nottingham, U.K., in 2012, and the Ph.D. degree in electrical and electronics engineering from the University of Sheffield, Sheffield, U.K., in 2016.

He is currently an Associate Professor with the Engineering Faculty, Kirsehir Ahi Evran University, Kirsehir, Turkey. His research interest includes advanced control strategies for ac drives.

**Yimin Zhou** (Member, IEEE) received the Ph.D. degree in control engineering from the University of Oxford, Oxford, U.K., in 2008.

She is currently a Professor with the Shenzhen Institutes of Advanced Technology, Chinese Academy of Sciences, Shenzhen, China. Her current research interests include optimal control, fault diagnosis, neuro-fuzzy modeling, machine learning, and energy management.